Rigorous Combined Mode-Matching Integral Equation Analysis of Horn Antennas with Arbitrary Cross Section

Rainer Bunger, *Member, IEEE*, Ralf Beyer, and Fritz Arndt, *Fellow, IEEE*

***Abstract*— A combined rigorous method is presented for the analysis of horn antennas with arbitrary cross section and general outer surface. The horn taper is described by the mode-matching (MM) method where the cross-section eigenvalue problem is solved by a two-dimensional (2-D) finite element (FE) technique. For the exterior horn surface including the radiating aperture, the application of the Kirchhoff–Huygens principle yields two expressions for the admittance matrix which are based on the electric (EFIE) and the magnetic (MFIE) field integral equation, respectively. The equations are solved numerically by the method of moments (MoM). For the preferred EFIE formulation, the eigenvectors of the last waveguide taper section and RWG functions for triangular patches are utilized as basis-functions for the magnetic or electric surface current densities, respectively. The presented method is verified by available reference values or measurements for a waveguide radiator with a peripheral choke, a conical and a rectangular horn. Its flexibility is demonstrated at the example of a conical ridged waveguide horn.**

***Index Terms*— Horn antennas, integral equation methods, method of moments, mode-matching methods.**

I. Introduction

WAVEGUIDE horn antennas have been explored for a long time for a wide variety of applications both as direct radiators and as feeds for reflectors [1]–[15]. The simulation models for numerical horn investigations can be categorized mainly in three types: 1) the aperture is assumed to be terminated in a large waveguide and the radiation pattern is computed by field integration, e.g., [1], [2], and [5]; 2) an infinite screen is assumed to be placed in the aperture plane, e.g., [4], [6], and [7]; and 3) more rigorous analyses reported in [8]–[15], which take the outer horn surface into account. The present paper belongs to category 3).

Complete three-dimensional (3-D) models for the overall outer *and* inner horn structure (based on pure integral equation methods [9], [10], [13] or finite-difference techniques [11]) are rather flexible, but the high numerical effort usually required for accurate results is considered to limit often their practical applicability. The mode-matching (MM) techniques of [14] and [15] are more efficient; the outer surface, however, is restricted to a spherical segment [14] or to structures with symmetry of revolution [15]. Preferable hybrid MM integral equation approaches are confined to circular [8] or rectangular horns [12] so far.

This paper applies a combined MM integral equation method to the more general case of horns with arbitrary shape concerning both the interior cross sections and the outer geometry. In contrast to the two–dimensional (2-D) formulations at bodies of revolution in [8], for the 3-D structures to be investigated in this paper, the standard combined source integral equation (CSIE) approach would lead to unphysical line charges and, hence, alternative electric field integral equation (EFIE) and magnetic field integral equation (MFIE) formulations are required. In comparison with the rooftop basis function approach for the rectangular case in [12], more universal Rao–Wilton–Glisson (RWG) functions [22] for the advantageous triangular patch modeling are utilized. Moreover, the whole interior taper structure is modeled by the combined mode-matching finite-element (MM FE) method of [16] and [17], which yields immediately the overall modal scattering matrix.

As a small aperture example, a radiating waveguide with a peripheral choke is investigated and compared with reference calculations. For further verification purposes, a conical and a rectangular horn are calculated and compared with available measurements. The flexibility of the presented method is demonstrated at the example of a conical ridged waveguide horn (Fig. 1).

II. Theory

The analysis is subdivided in three calculation steps. In the first step (cf. Fig. 2), the method of moments (MoM) is applied to calculate the modal scattering matrices of the waveguide aperture (with the cross section of the last section of the horn taper) and of the outer geometry of the horn antenna. The eigenvectors of the last horn taper section are computed by the FE approach [16] or are known analytically.

In the second step, the scattering matrix of the interior horn taper is computed with the MM method of [17].

The third step comprises the calculation of the total scattering matrix composed of the known modal-scattering matrix of the interior horn taper and the modal-scattering matrix of the aperture. The amplitudes of the forward and backward propagating modes in the last section of the taper yield the magnetic and electric surface current densities in terms of the corresponding basis functions.

Manuscript received April 7, 1998; revised October 29, 1998.

The authors are with Microwave Department, University of Bremen, D-28334 Bremen, Germany.

Publisher Item Identifier S 0018-926X(99)09942-1.

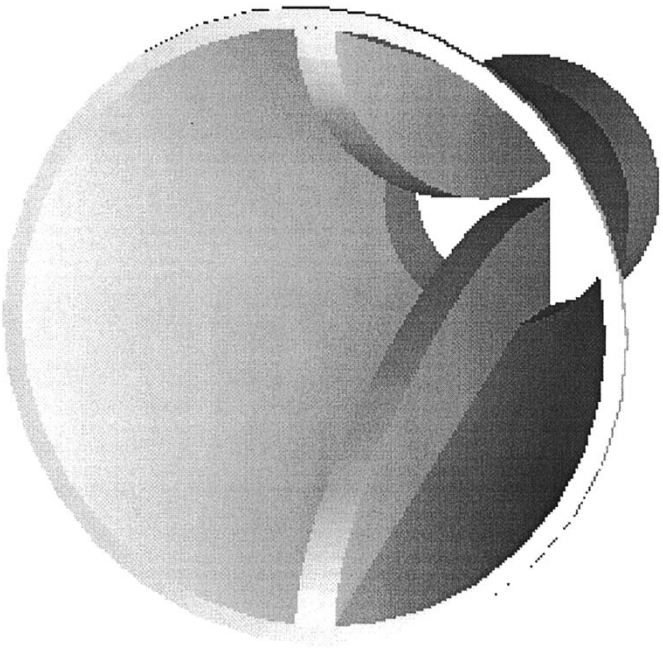

Fig. 1. Ridged waveguide horn antenna.

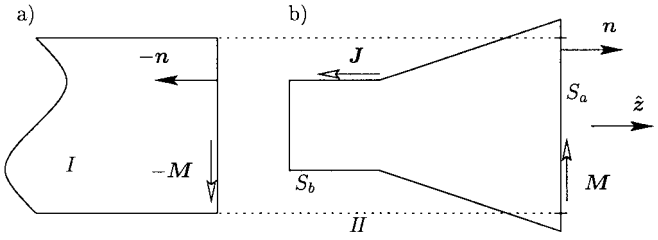

Fig. 2. Model for the first step of the analysis. (a) Subproblem for the waveguide—region *I*. (b) Subproblem for region *II*.

A. Method of Moments

According to [18], the entire structure is subdivided into two regions, the inner (*I*) and the outer region (*II*), cf. Fig. 2. Both regions are separated by a perfectly conducting surface S_a. In order to maintain the original problem, magnetic surface current densities are introduced which restore the tangential electric field on the surface S_a.

Enforcing the continuity of the tangential magnetic field on the aperture yields the following equation for the magnetic surface current density:

$$\mathbf{H}_{\tan}^{\text{inc}} = \mathbf{H}_{\tan}^{I}(\mathbf{M}) + \mathbf{H}_{\tan}^{II}(\mathbf{M}) \quad \text{on } S_a \tag{1}$$

where $\mathbf{H}_{\tan}^{\text{inc}}$, $\mathbf{H}_{\tan}^{I}(\mathbf{M})$, and $\mathbf{H}_{\tan}^{II}(\mathbf{M})$ are the tangential incident magnetic field in region *I*, the linear operator for the tangential scattered magnetic field in region *I* and the linear operator for the tangential scattered magnetic field in region *II*, respectively.

1) Region I: For the solution of (1), the MoM is employed. The magnetic surface current density is approximated by Q linear independent basis functions $\mathbf{M}_q$ on S_a

$$\mathbf{M}(\mathbf{r}) = \eta_0 \sum_{q=1}^{Q} V_q \mathbf{M}_q(\mathbf{r}), \quad \mathbf{r} \text{ on } S_a \tag{2}$$

where the V_q are the expansion coefficients for the magnetic surface current density. η_0 denotes the free-space impedance. Introducing a set of $P = Q$ linear independent test functions $\mathbf{W}_p$ on S_a results in a system of linear equations (see Appendix A).

2) Region II: The calculation of the admittance matrix for the outer geometry is based on the Kirchhoff–Huygens principle, cf. [25]. The electromagnetic field in region *II* is calculated using the electric surface current densities on S_a and S_b and the magnetic surface current densities on S_a

$$\mathbf{M}(\mathbf{r}) = \begin{cases} -\mathbf{n} \times \mathbf{E}(\mathbf{r}) & \mathbf{r} \text{ on } S_a \\ 0 & \mathbf{r} \text{ on } S_b, \end{cases} \tag{3a}$$

$$\mathbf{J}(\mathbf{r}) = \mathbf{n} \times \mathbf{H}(\mathbf{r}), \quad \mathbf{r} \text{ on } S_a \text{ or } S_b. \tag{3b}$$

The electromagnetic field in region *II* is written as

$$\mathbf{E}(\mathbf{r}) = -\text{rot} \int_S \mathbf{M}(\mathbf{r}') G_0(\mathbf{r}, \mathbf{r}')\, dS' + \frac{1}{j\omega\epsilon_0} \text{rot}\,\text{rot} \int_S \mathbf{J}(\mathbf{r}') G_0(\mathbf{r}, \mathbf{r}')\, dS' \tag{4a}$$

$$\mathbf{H}(\mathbf{r}) = \text{rot} \int_S \mathbf{J}(\mathbf{r}') G_0(\mathbf{r}, \mathbf{r}')\, dS' + \frac{1}{j\omega\mu_0} \text{rot}\,\text{rot} \int_S \mathbf{M}(\mathbf{r}') G_0(\mathbf{r}, \mathbf{r}')\, dS' \tag{4b}$$

with the Green's function for the potential in free-space

$$G_0(\mathbf{r}, \mathbf{r}') = \frac{1}{4\pi} \frac{e^{-jk_0|\mathbf{r}-\mathbf{r}'|}}{|\mathbf{r}-\mathbf{r}'|}. \tag{4c}$$

The magnetic and electric surface current densities are expanded in (2) and

$$\mathbf{J}(\mathbf{r}) = \sum_{s=1}^{S} I_s \mathbf{J}_s(\mathbf{r}), \quad \mathbf{r} \text{ on } S_a \text{ or } S_b \tag{5}$$

respectively. The tangential electric and magnetic fields and the electric and magnetic surface current densities in (4a) and (4b) are replaced by (2) and (5). As (4a) and (4b) can be used independently, two different expansion expressions for the two equations are introduced which are distinguished in their notation by single [belonging to (4a)] and double primes [belonging to (4b)], respectively. The tangential fields are related with the surface current densities by (3a) and (3b). After introducing a set of R', R'' linear independent test functions $\mathbf{U}_r'$, $\mathbf{U}_r''$ both on S_a and S_b, respectively, as well as inner products of $\mathbf{U}_r'$, $-\mathbf{n} \times \mathbf{U}_r''$ and (4a), (4b), respectively, two systems of linear equations are derived [25] (see Appendix B).

From these equations and (12a) and (12b), the following two different expressions for the admittance matrix for region *II* result:

$$\left[T_{pq}^{\prime II}\right] = \left[F_{ps}^{J}\right]\left[T_{rs}^{J}\right]^{-1}\left[D_{rq}^{M} - S_{rq}^{M}\right] \tag{6a}$$

$$\left[T_{pq}^{\prime\prime II}\right] = \left[F_{ps}^{J}\right]\left[D_{rs}^{J} - S_{rs}^{J}\right]^{-1}\left[T_{rq}^{M}\right]. \tag{6b}$$

Equations (6a) and (6b) are basically the electric and magnetic field equations EFIE and MFIE.[1]

[1]Although the EFIE is preferred for the numerical calculations in our paper, both formulations are presented for a more thorough elucidation of the advantageous choice of basis functions, see Section III-A

3) Calculation of the Aperture Scattering Matrix: Using the orthonormality of the eigenvectors [cf. (10)], the following expression for the elements of the modal scattering matrix of the aperture is derived by assuming that the amplitudes of all incident modes are equal to one

$$s_{ij} = -\eta_0 \sum_{q=1}^{Q} A_{iq} V_{qj} - \delta_{ij} \tag{7}$$

where V_{qj} is the expansion coefficient for the basis function $\mathbf{M}_q$ for excitation with mode j only.

B. Modal Scattering Matrix of the Interior Horn Taper

In the second calculation step, the modal-scattering matrix of the interior horn taper is computed with a MM method [17], where the cross-section eigenvalue problem for not analytically solvable structures is calculated by a 2-D FE technique [16]. All basic relations are well documented in [16] and [17], the reader is referred, therefore, to the corresponding literature.

C. Analysis of the Complete Structure

In the third calculation step, we combine the modal-scattering matrix of the taper with that of the aperture [(7), after applying the possible normalization]. The results are the overall modal scattering matrix of the complete structure (as seen from the feeding waveguide port) and the forward and backward propagating wave amplitudes in the last section of the horn taper. The amplitudes of the forward waves are used to set up new incident current vectors $[I^{\text{inc}}]$. Using the already computed matrices, voltage and current vectors are obtained for the magnetic and electric surface current densities. The far field is then calculated via (4a) and (4b).

III. Implementation

A. Adequate Choice of the Basis and Test Functions

Our investigations and those in [20] and [21] have shown that the choice of basis functions for the electric and magnetic surface current densities is critical: in this formulation, the utilization of the RWG basis functions $\mathbf{f}$ [22] for *both* the electric *and* the magnetic surface current density would result in a numerically singular matrix $[T^I + T^{II}]$.

Because of the evaluation of the T^M and T^J matrix in mixed potential form [(6a) and (6b)], not only the divergence of the basis functions but also the divergence of the test functions are involved. For the EFIE, we need the divergence of $\mathbf{U}'_r$, for the MFIE that of $-\mathbf{n} \times \mathbf{U}''_r$. The adequate choice of basis functions, therefore, depends on whether the EFIE or MFIE [i.e., (6a) or (6b)] is applied for the admittance matrix formulation of region *II*.

For the EFIE, an advantageous choice is to take the set of the $-\mathbf{u}_z \times \mathbf{e}_i$ of region *I* as basis functions for the magnetic surface current densities. Because of their orthonormality, the admittance matrix $[T^I]$ and the incident current vectors $[I^{\text{inc}}]$ are given in analytical form. Since the divergence of these basis functions is not involved, numerically available eigenvectors can be used directly. A further advantage is that the matrices $[S^M]$ and $[D^M]$ include commonly only a rather small number of columns (depending on the number of modes considered for the calculation of the last horn taper

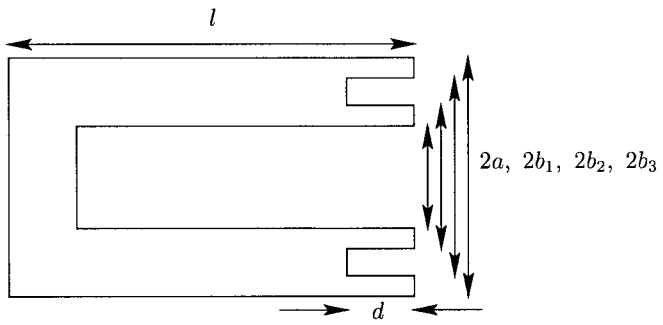

(a)

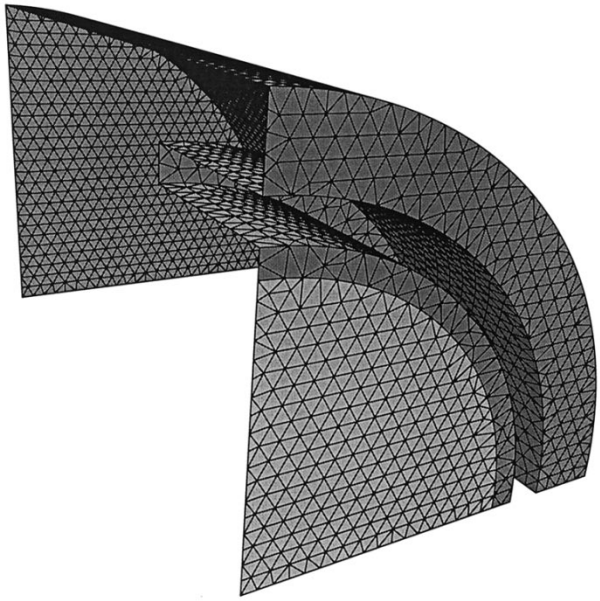

(b)

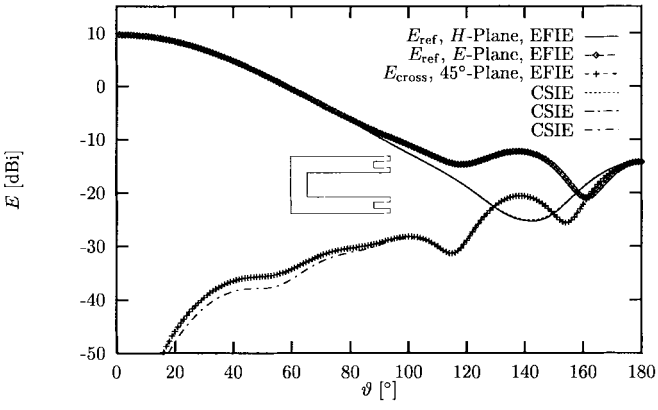

(c)

Fig. 3. (a) Radiating waveguide with a peripheral choke [25]. Dimensions: $a = 11.5$ mm, $b_1 = 12.5$ mm, $b_2 = 14$ mm, $b_3 = 17$ mm, $d = 7.5$ mm, $l = 29$ mm. (b) Discretization of the radiator with triangular elements. (c) Far-field pattern for $f = 10.5$ GHz. Comparisons of the results of the present method (EFIE) with own calculations (CSIE) by applying the method of [25] for bodies of revolution.

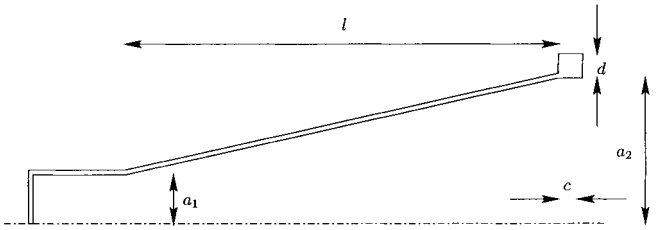

(a)

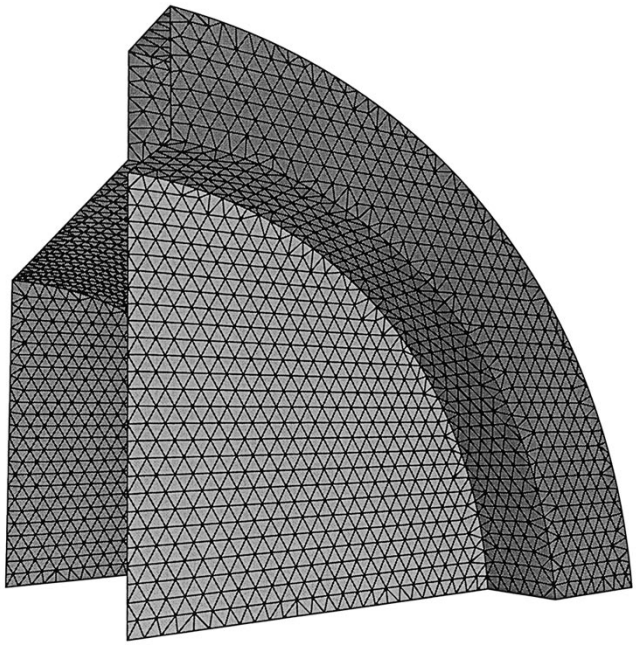

(b)

Fig. 4. (a) Conical waveguide horn antenna. Dimensions: $a_1 = 9$ mm, $a_2 = 35$ mm, $c = 8.2$ mm, $d = 10$ mm, $l = 302.5$ mm. (b) Discretization of the conical horn antenna with triangular elements.

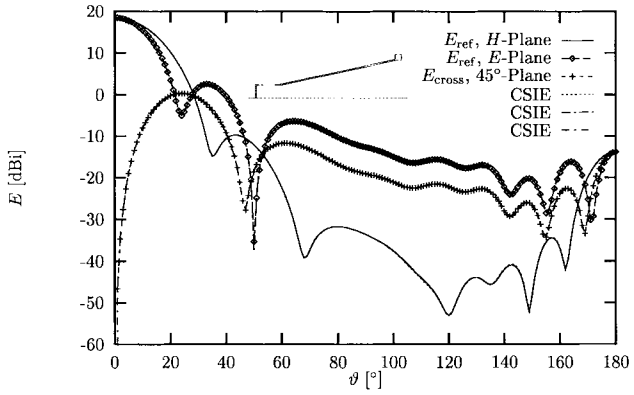

(a)

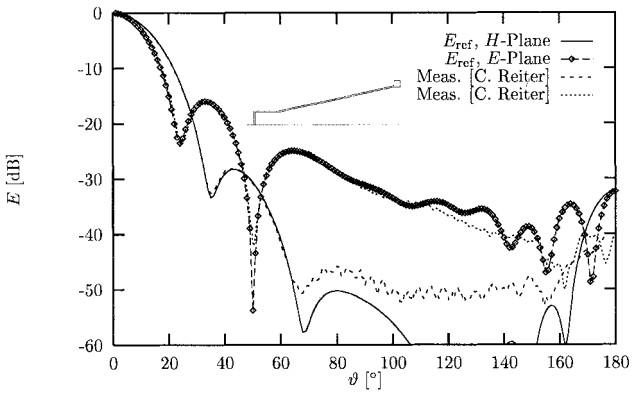

(b)

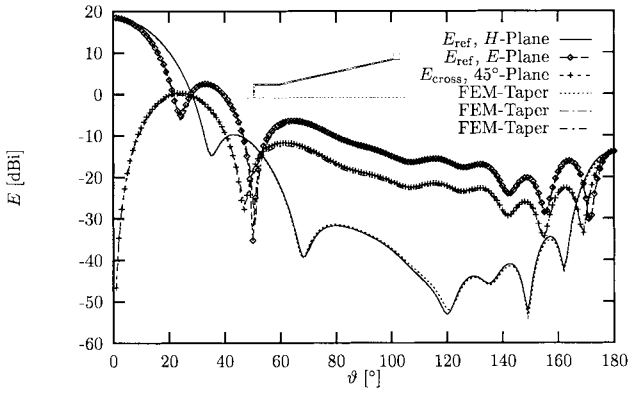

(c)

Fig. 5. (a) Far field of the conical horn in Fig. 4(a) for a frequency $f = 12.5$ GHz. Comparison of the present method with own calculations applying a combined source integral equation (CSIE) approach for bodies of revolution (BOR). (b) Comparison of the present method with measurements. (c) Comparison of the present method using analytical and numerical eigenvectors.

section). For the electric surface current densities, the RWG basis functions [22] for triangular patches are well appropriate.

When applying the MFIE, a selection of RWG basis functions in the form $\mathbf{n}\times\mathbf{f}$ for the electric surface current densities is suitable. Also here, their divergence is not involved. Because of the $\mathbf{n}\times$ operation required for the RWG basis functions, however, their usual positive attributes vanish: this set does not meet any more the boundary conditions for the electric surface current density on open surfaces automatically and it produces line charges.

Therefore, the EFIE is preferred for the calculations in this paper. As for the test functions according to the chosen Galerkin method, the $P = Q$ functions $\mathbf{W}_p$ are the basis functions for the magnetic surface current density $\mathbf{M}_q$; the $R = S$ functions $\mathbf{U}_r$ are those for the electric surface current density $\mathbf{J}_s$.

B. Evaluation of the MoM Integrals

The T-matrix elements are transformed into the well-known mixed potential form in order to have a $1/R$ singularity only. These singularities have been integrated analytically with the help of the formulas developed in [23]. The remaining numerical integrations are evaluated in normalized area coordinates according to [22] using a three- and a seven-point rule [24].

The correct evaluation of the S-matrix elements requires the separation of the source point integral into a Cauchy principal value term and a residue term in the usual way.

Applicable symmetries are fully utilized in order to reduce the memory and central processing unit (CPU) time requirements. For this purpose, the corresponding basis functions are supplemented by additional images of themselves, which replace the symmetry walls accordingly.

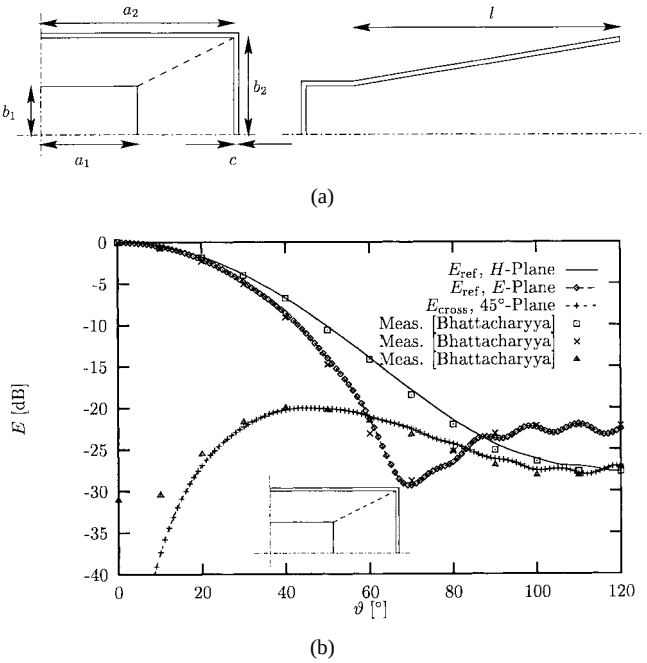

Fig. 6. (a) Rectangular waveguide horn antenna [7]. Dimensions: $a_1 = 7.8994$ mm, $b_1 = 3.9497$ mm, $a_2 = 12.7$ mm, $b_2 = 11.43$ mm, $l = 101.6002$ mm, $c = 1.016$ mm. (b) Comparison of the present approach with measured reference values of [7] for a frequency $f = 13.997$ GHz.

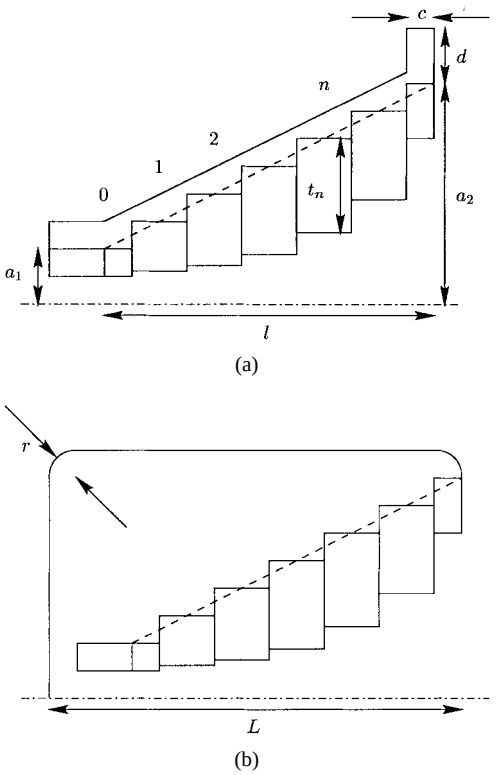

Fig. 7. (a) Conical ridged waveguide horn antenna. Dimensions: $a_1 = 30.0875$ mm, $a_2 = 75.38$ mm, $c = 3$ mm, $d = 10$ mm. $l = 180$ mm. The width of the ridges is $w = 10$ mm. The parameters t_n for each section of the taper are given in the appendix. (b) Conical ridged waveguide horn antenna with rounded corners. Dimensions of the outer geometry: $L = 160$ mm, $r = 10$ mm. Other dimensions as in Fig. 7(a).

IV. Results

First, as a small aperture example, a radiating waveguide with a peripheral choke [Fig. 3(a) and (b)] is investigated and compared with own reference calculations by applying the method of [25] for bodies of revolution [Fig. 3(c)]. Although a locally rather coarse discretization has been used for the present method (the side lengths of the triangular patches [cf. Fig. 3(b)] are already in the order of the smallest geometrical dimensions),[2] only slight deviations can be observed at the cross-polarization pattern in the lower level range.

For reference purposes with available measurements, a circular horn structure [15] is investigated. Fig. 4(a) shows the geometry of the horn, Fig. 4(b) illustrates the surface mesh of one quarter of the structure used for the moment method solution as well as the area S_a that separates the regions *I* and *II*. The radiation field is plotted in Figs. 5. Good agreement with own reference calculations using a combined source integral equation (CSIE) method according to [8] [Fig. 5(a)] and with measurements [15] [Fig. 5(b)] may be stated. Fig. 5(c) shows the the results obtained by using the analytical solution of the circular horn taper eigenvalue problem compared with the corresponding 2-D FE solution.

The second reference structure where measurements are available is a rectangular horn according to [7] (Figs. 6).

To demonstrate the flexibility of the presented method, a ridged horn structure (Figs. 1, 7, 8) is investigated. The ridged horn taper section [Fig. 7(a)] has been optimized with regard to a high bandwidth of the input return loss [16]. In order to enable reference calculations with the boundary contour spherical wave expansion (SWE) MM technique [15], first the outer contour of the horn is shaped according to Fig. 7(b). The result is plotted in Fig. 8(a).

For checking the convergence properties of the formulation in this paper, the ridged horn structure [Fig. 7(a)] has been simulated with different numbers of triangles and modes at $f = 5.02$ GHz. For the first simulation run the mesh size was 3 mm, resulting in a total number of 4970 triangles. Thirty-two modes on the aperture have been used. The mesh size has been increased to 9 mm for the second simulation run. This corresponds to merely 595 triangles on S_a and S_b. Twenty-four modes on the aperture have been considered. It turned out that the differences in the far field for the two different simulations are less than 0.1 dB. It is worth to note that the mesh size of the coarse mesh in the second simulation run is larger than the smallest dimension of the structure.

For Fig. 8(b)–(d), the outer contour is shaped more realistically according to Fig. 7(a). Fig. 8(b)–(d) shows the radiation pattern for different frequencies. The comparison of Figs. 8(a) and (c) ($f = 5.02$ GHz) reveals the noticeable difference in the radiation pattern for the different outer contours according to Figs. 7(b), and (a), respectively.

In Fig. 8(e), the overall return loss in the feed waveguide of the complete horn is plotted against frequency which demonstrates the rather large bandwidth of such structures.

[2] Note that the choke is rather deep compared to the front dimensions of the waveguide [cf. Fig. 3(b)] and the current densities at the front side are of high influence on the cross-polarization level.

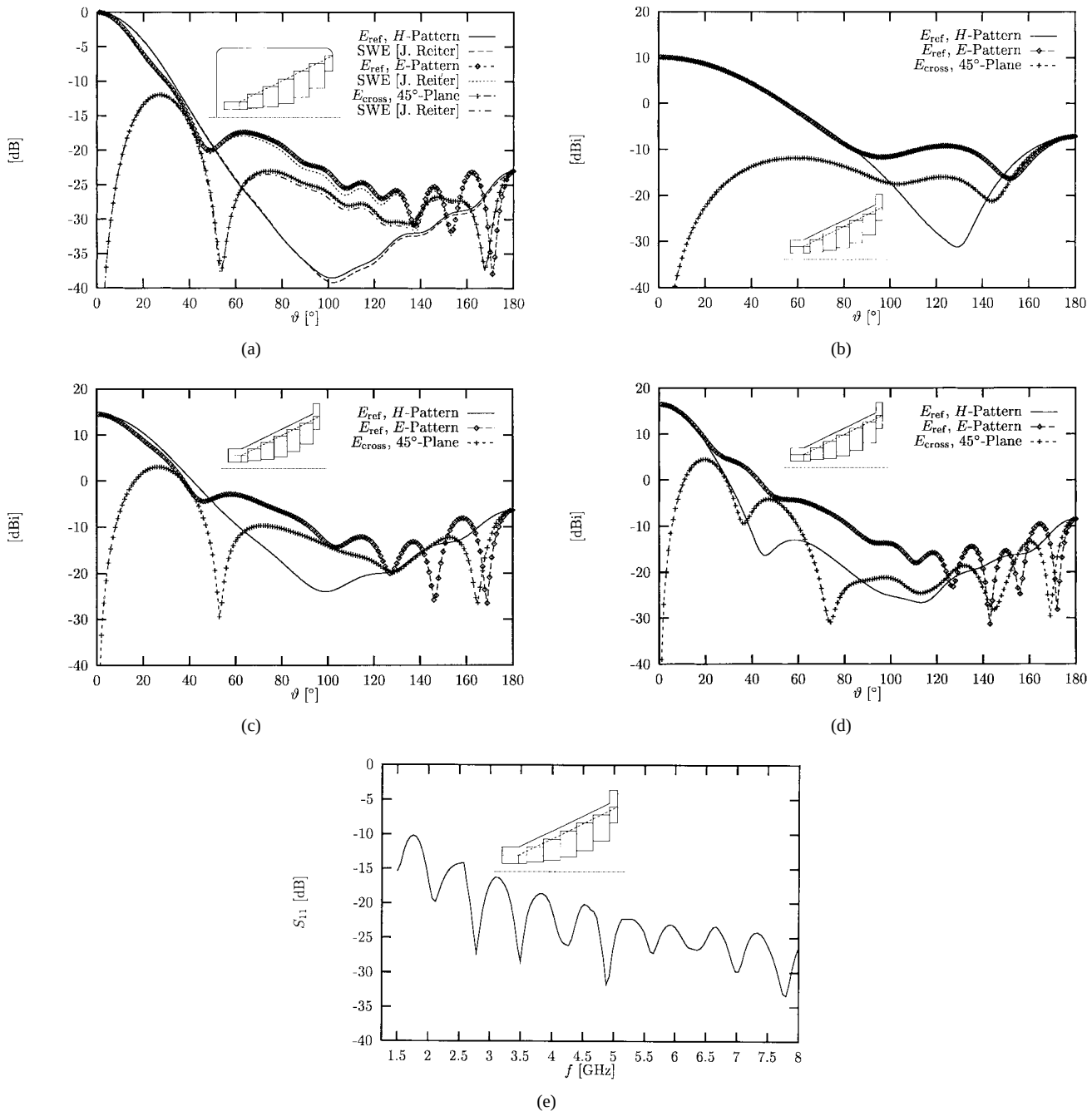

Fig. 8. (a) Far field of the antenna in Fig. 7(b). Comparison of the present approach with a spherical wave expansion for a frequency $f = 5.02$ GHz. (b) Far field of the antenna of Fig. 7(a) for a frequency $f = 2$ GHz. (c) Far field of the antenna of Fig. 7(a) for a frequency $f = 5.02$ GHz. (d) Far field of the antenna of Fig. 7(a) for a frequency $f = 7$ GHz. (e) Scattering parameter S_{11} of the fundamental mode in the feed waveguide as a function of the frequency for the structure in Fig. 7(a).

V. Conclusion

A flexible hybrid method is presented for the rigorous analysis of horn antennas of arbitrary interior cross section and general outer surface. The horn taper transition is modeled by the modal scattering matrix based on the MM method. For the outer surfaces of the horn including the radiating aperture, the Kirchhoff–Huygens principle is applied. The resulting integral equations are solved numerically by the MoM. The accuracy of the method is verified by comparisons with reference calculations or measurements. The analysis of a conical-ridged waveguide horn demonstrates the flexibility of the method.

Appendix A
Equations for Region I

$$\left[I_{pj}^{\text{inc}}\right] = \left[T_{pq}^{I} + T_{pq}^{II}\right]\left[V_{qj}\right] \tag{8a}$$

with

$$\left[I_{pj}^{\text{inc}}\right] = \left[\left\langle \mathbf{W}_p; \mathbf{H}_{\tan}^{\text{inc},j}\right\rangle\right] \tag{8b}$$

$$\left[T_{pq}^{I}\right] = \left[\eta_0\left\langle \mathbf{W}_p; \mathbf{H}_{\tan}^{I}(\mathbf{M}_q)\right\rangle\right] \tag{8c}$$

$$\left[T_{pq}^{II}\right] = \left[\eta_0\left\langle \mathbf{W}_p; \mathbf{H}_{\tan}^{II}(\mathbf{M}_q)\right\rangle\right] \tag{8d}$$

and the inner products defined as

$$\langle \mathbf{A}; \mathbf{B}\rangle = \int_S \mathbf{A}\cdot\mathbf{B}\, dS. \tag{8e}$$

In this approach, $[T^I]$ is the admittance matrix of a waveguide of infinite length with S_a as cross-section surface. The elements of the waveguide admittance matrix are defined as [19]

$$T^I_{pq} = -\eta_0 \sum_{i=1}^{I} B_{pi} Y_i A_{iq} \tag{9a}$$

with

$$A_{iq} = \int_S \mathbf{M}_q \cdot \left(\hat{\mathbf{z}} \times \mathbf{e}_i\right) dS \tag{9b}$$

$$B_{pi} = \int_S \mathbf{W}_p \cdot \left(\hat{\mathbf{z}} \times \mathbf{e}_i\right) dS \tag{9c}$$

and the TE and TM eigenvectors of the waveguide $\mathbf{e}_i$ and their modal admittances Y_i. The normalization for the eigenvectors is

$$\int_{S_a} \mathbf{e}_i \cdot \mathbf{e}_j \, dS = \delta_{ij} = \begin{cases} 1 & i = j, \\ 0 & i \neq j. \end{cases} \tag{10}$$

APPENDIX B
EQUATIONS FOR REGION *II*

$$\left[D^M_{rq}\right]\left[V'_q\right] = \left[S^M_{rq}\right]\left[V'_q\right] + \left[T^J_{rs}\right]\left[I'_s\right] \tag{11a}$$

$$\left[D^J_{rs}\right]\left[I''_s\right] = \left[S^J_{rs}\right]\left[I''_s\right] + \left[T^M_{rq}\right]\left[V''_q\right] \tag{11b}$$

with

$$S^M_{rq} = \left\langle \mathbf{U}'_r; -\mathrm{rot} \int_{S_a} \mathbf{M}'_q G_0 \, dS' \right\rangle \tag{11c}$$

$$T^J_{rs} = \frac{1}{jk_0} \left\langle \mathbf{U}'_r; \mathrm{rot}\,\mathrm{rot} \int_{S_a+S_b} \mathbf{J}'_s G_0 \, dS' \right\rangle \tag{11d}$$

$$S^J_{rs} = \left\langle -\mathbf{n} \times \mathbf{U}''_r; \mathrm{rot} \int_{S_a+S_b} \mathbf{J}''_s G_0 \, dS' \right\rangle \tag{11e}$$

$$T^M_{rq} = \frac{1}{jk_0} \left\langle -\mathbf{n} \times \mathbf{U}''_r; \mathrm{rot}\,\mathrm{rot} \int_{S_a} \mathbf{M}''_q G_0 \, dS' \right\rangle \tag{11f}$$

$$D^M_{rq} = \langle \mathbf{U}'_r; \mathbf{n} \times \mathbf{M}'_q \rangle \tag{11g}$$

$$D^J_{rs} = \langle -\mathbf{n} \times \mathbf{U}''_r; -\mathbf{n} \times \mathbf{J}''_s \rangle \tag{11h}$$

where the arguments are omitted far the sake of brevity. Vectors $[V_q]$ and $[I_s]$ denote a column of their corresponding matrices for a excitation with a single mode j only. Both systems of linear equations can be solved for the current vector $[I_s]$

$$\left[I'_s\right] = \left[T^J_{rs}\right]^{-1}\left[D^M_{rq} - S^M_{rq}\right]\left[V'_q\right] \tag{12a}$$

$$\left[I''_s\right] = \left[D^J_{rs} - S^J_{rs}\right]^{-1}\left[T^M_{rq}\right]\left[V''_q\right]. \tag{12b}$$

Utilizing now the linearity of the operator $\mathbf{H}^{II}$ and (3b), the following expression can be derived:

$$\eta_0 \sum_{q=1}^{Q} V_q \left\langle \mathbf{W}_p; \mathbf{H}^{II}_{\tan}(\mathbf{M}_q) \right\rangle = \sum_{s=1}^{S} I_s \langle \mathbf{W}_p; -\mathbf{n} \times \mathbf{J}_s \rangle \qquad p = 1, \ldots, P. \tag{13}$$

Introducing the matrix

$$\left[F^J_{ps}\right] = \left[\langle \mathbf{W}_p; -\mathbf{n} \times \mathbf{J}_s \rangle\right] \tag{14}$$

one can write

$$\left[T^{II}_{pq}\right]\left[V_q\right] = \left[F^J_{ps}\right]\left[I_s\right]. \tag{15}$$

Equations (6a) and (6b) are derived from this equation (cf. [25]).

APPENDIX C

TABLE I
GEOMETRY OF THE RIDGED WAVEGUIDE TAPER IN FIGS. 7 AND 8

Section number	t [mm]	Section number	t [mm]
0	26.83		
1	27.30	31	31.44
2	27.76	32	31.22
3	28.20	33	31.00
4	28.62	34	30.79
5	29.02	35	30.53
6	29.40	36	30.22
7	29.75	37	29.88
8	30.08	38	29.51
9	30.40	39	29.10
10	30.68	40	28.67
11	30.94	41	28.24
12	31.18	42	27.81
13	31.40	43	27.33
14	31.60	44	26.80
15	31.78	45	26.22
16	31.92	46	25.63
17	32.04	47	24.93
18	32.15	48	24.15
19	32.23	49	23.35
20	32.28	50	22.50
21	32.32	51	21.60
22	32.33	52	20.60
23	32.33	53	19.50
24	32.32	54	18.30
25	32.24	55	16.80
26	32.16	56	15.00
27	32.08	57	13.00
28	32.00	58	10.50
29	31.84	59	7.50
30	31.66	60	0.00

ACKNOWLEDGMENT

The authors would like to thank C. Reiter for providing the measurements of the conical reference horn. They would also like to thank J. Reiter for many helpful discussions.

REFERENCES

[1] A. D. Olver, P. J. B. Clarricoats, A. A. Kishk, and L. Shafai, *Microwave Horns and Feeds*. New York: IEEE, Press, 1994.
[2] B. M. A. Thomas, G. L. James, and K. J. Greene, "Design of wide-band corrugated conical horns for cassegrain antennas," *IEEE Trans. Antennas Propagat.*, vol. AP-34, pp. 750–757, June 1986.
[3] A. D. Olver and J. Xiang, "Design of profiled corrugated horns," *IEEE Trans. Antennas Propagat.*, vol. 36, pp. 936–940, July 1988.
[4] J. A. Encinar and J. M. Rebollar, "A hybrid technique for analyzing corrugated and noncorrugated horns," *IEEE Trans. Antennas Propagat.*, vol. AP-34, pp. 961–968, Aug. 1986.
[5] F. Arndt, U. Papziner, and R. Bohl, "Field theory CAD of profiled corrugated rectangular or circular horns by an efficient full-wave modal-S-matrix method," in *IEEE AP-S Int. Symp. 1993 Dig.*, Ann Arbor, MI, June/July 1993, vol. 2, pp. 1026–1029.
[6] T. Wriedt, K. H. Wolff, F. Arndt, and U. Tucholke, "Rigorous hybrid field theoretic design of stepped rectangular waveguide mode converters including the horn transitions into half-space," *IEEE Trans. Antennas Propagat.*, vol. 37, pp. 780–790, June 1989.

[7] A. K. Bhattacharyya and G. Z. Rollins, "Accurate radiation and impedance characteristics of horn antennas—A moment method model," *IEEE Trans. Antennas Propagat.*, vol. 44, pp. 523–531, Apr. 1996.
[8] E. Kühn and V. Hombach, "Computer-aided analysis of corrugated horns with axial ring or ring-loaded radial slots," in *Proc. ICAP 83—Pt. I*, U.K., Mar. 1983, pp. 127–131.
[9] L. Botha and D. A. McNamara, "Examination of antenna patterns of profiled horns using the method of moments," in *IEEE AP-S Int. Symp. 1985 Dig.*, Vancouver, Canada, June 1985, vol. 1, pp. 293–296.
[10] M. F. Catedra, "Analysis of bodies of revolution composed of conductors and dielectrics using only electric equivalent currents: Application to small horns with dielectric core," *IEEE Trans. Antennas Propagat.*, vol. 36, pp. 1311–1313, Sept. 1988.
[11] P. A. Tirkas and C. A. Balanis, "Finite-difference time-domain method for antenna radiation," *IEEE Trans. Antennas Propagat.*, vol. 40, pp. 334–340, Mar. 1992.
[12] K. Liu, C. A. Balanis, C. R. Birtcher, and G. C. Barber, "Analysis of pyramidal horn antennas using moment methods," *IEEE Trans. Antennas Propagat.*, vol. 41, pp. 1379–1389, Oct. 1993.
[13] P. Ratajczak, P. Brachat, and J.-L. Guiraud, "Rigorous analysis of three-dimensional structures incorporating dielectrics," *IEEE Trans. Antennas Propagat.*, vol. 42, pp. 1077–1088, Aug. 1994.
[14] R. R. Collmann and F. M. Landstorfer, "Calculation of the field radiated by horn-antennas using the mode-matching method," *IEEE Trans. Antennas Propagat.*, vol. 43, pp. 876–880, Aug. 1995.
[15] J. M. Reiter and F. Arndt, "Efficient hybrid boundary contour mode-matching technique for the accurate full-wave analysis of circular horn antennas including the outer wall geometry," *IEEE Trans. Antennas Propagat.*, vol. 45, pp. 568–570, Mar. 1997.
[16] R. Beyer and F. Arndt, "Efficient modal analysis of waveguide filters including the orthogonal coupling elements by an MM/FE method," *IEEE Microwave Guided Wave Lett.*, vol. 5, pp. 9–11, Jan. 1995.
[17] F. Arndt, R. Beyer, J. M. Reiter, T. Sieverding, and T. Wolf, "Automated design of waveguide components using hybrid mode-matching/numerical EM building-blocks in optimization oriented CAD frame-works—State-of-the-art and recent advances," *IEEE Trans. Microwave Theory Tech.*, vol. 45, pp. 747–760, May 1997.
[18] J. R. Mautz and R. F. Harrington, "A generalized network formulation for aperture problems," *IEEE Trans. Antennas Propagat.*, vol. AP-24, pp. 870–873, Nov. 1976
[19] H. Auda and R. F. Harrington, "A moment solution for waveguide junction problems," *IEEE Trans. Microwave Theory Tech.*, vol. MTT-31, pp. 515–520, July 1983.
[20] T. K. Sarkar, S. M. Rao, and A. R. Djordjevic, "Electromagnetic scattering and radiation from finite microstrip structures," *IEEE Trans. Microwave Theory Tech.*, vol. 38, pp. 1568–1575, Nov. 1990.
[21] U. Jakobus and F. M. Landstorfer, "Novel basis function for the equivalent magnetic current in the method of moments solution of dielectric scattering problems," *Electron. Lett.*, vol. 29, pp. 1272–1273, July 1993.
[22] S. M. Rao, D. R. Wilton, and A. W. Glisson, "Electromagnetic scattering by surfaces of arbitrary shape," *IEEE Trans. Antennas Propagat.*, vol. AP-30, pp. 409–418, May 1982.
[23] D. R. Wilton, S. M. Rao, A. W. Glisson, D. H. Schaubert, O. M. Al-Bundak, and C. M. Butler, "Potential integrals for uniform and linear source distributions on polygonal and polyhedral domains," *IEEE Trans. Antennas Propagat.*, vol. AP-32, pp. 276–281, Mar. 1984.
[24] P. C. Hammer, O. P. Marlowe, and A. H. Stroud, "Numerical integration over simplexes and cones," *Math. Tables Aids Comp.*, vol. 10, pp. 130–137, 1956.
[25] V. Hombach, "Kreuzpolarization vor Hohlleitungsstrahlern," Ph.D. dissertation, Univ. Bochum, Germany, 1981.

Rainer Bunger (M'93) received the Dipl.-Ing. and the Dr.-Ing. degrees from the University of Bremen, Germany, in 1992 and 1997, respectively.

After a short stay at the Technical University Darmstadt, Germany, he continued working on numerical techniques for the solution of electromagnetic field problems at the University of Bremen, Germany, in 1998. His research interests include the method of moments, the fast multipole method, and the finite-difference time-domain technique.

Ralf Beyer, photograph and biography not available at the time of publication.

Fritz Arndt (SM'83–F'93) received the Dipl.-Ing., Dr.-Ing., and Habilitation degrees from the Technical University of Darmstadt, Germany, in 1963, 1968, and 1972, respectively.

From 1963 to 1972 he worked on directional couplers and microstrip techniques at the Technical University of Darmstadt. Since 1972 he has been a Professor and Head of the Microwave Department of the University of Bremen, Germany. His research activities are in the area of the solution of field problems of waveguide, finline, and optical waveguide structures, of antenna design, and of scattering structures.

Dr. Arndt is a member of the VDE and NTG (Germany). He received the NTG Award in 1970, the A. F. Bulgin Award (together with three coauthors) from the Institution of Radio and Electronic Engineers in 1983, and the Best Paper Award of the Antenna Conference JINA 1986 (France).